Publ. Astron. Soc. Japan (2017) 00 (0), 1–12
doi: 10.1093/pasj/psx049
Advance Access Publication Date: 2017 0

Photometric studies for two contact binaries: V532 Monocerotis and GU Orionis

Yuangui Yang,[1,*] Haifeng Dai,[1,*] Huiyu Yuan,[1] Xiliang Zhang,[2] and Liyun Zhang[3]

[1]Information College/School of Physics and Electronic Information, Huaibei Normal University, Huaibei 235000, Anhui Province, China
[2]Key Laboratory for the Structure and Evolution of Celestial Objects, Chinese Academy of Sciences, Kunming 650011, China
[3]Department of Physics and Astronomy, College of Physics, Guizhou University, Guiyang 550025, China

*E-mail: daihf@mail.ustc.edu.cn (HD); yygcn@163.com (YY)

Received 2016 February 12; Accepted 2017 May 23

Abstract

We present photometry and spectroscopy data for V532 Mon and GU Ori, observed in 2011 and 2016. From the spectral observations, the spectral types are determined to be F5V for V532 Mon and G0V for GU Ori. With the 2015-version Wilson–Devinney program, the photometric solutions are simultaneously deduced from *VR* light curves (LCs). The intrinsic variability for V532 Mon is found by comparing LCs in 2004 and 2011, while the asymmetric LCs for GU Ori are modeled by a cool spot on the more massive component. The results imply that the two stars are A-type contact binaries. The mass ratios and fill-out factors are, respectively, $q = 0.190(\pm0.006)$ and $f = 43.7(\pm0.9)\%$ for V532 Mon and $q = 0.455(\pm0.020)$ and $f = 26.9(\pm1.3)\%$ for GU Ori. From the $(O - C)$ curves, it is found that their orbital periods may be undergoing long-term variations. The rates of period change are $dP/dt = -1.72(\pm0.05) \times 10^{-7}\,\mathrm{d\,yr^{-1}}$ for V532 Mon and $dP/dt = +1.45(\pm0.01) \times 10^{-7}\,\mathrm{d\,yr^{-1}}$ for GU Ori. V532 Mon with a decreasing period will evolve into a deep-contact binary, while GU Ori with an increasing period may evolve into a broken-contact case.

Key words: binaries: close — binaries: eclipsing — stars: individual (V532 Monocerotis, GU Orionis)

1 Introduction

V532 Mon (= WDS 0720-0018) was discovered by Wachman (1966) as a variable star. Kukarkin et al. (1968) classified it as a W UMa-type binary with a period of 0.4670 d. Its visual magnitude ranges from 12.20 mag to 12.80 mag. The orbital period is $P = 0.4669759$ d (Kreiner 2004). Pribulla, Kreiner, and Tremko (2003) cataloged it as a field contact binary and suggested that its orbital period may be variable. Pribulla and Rucinski (2006) then listed it among contact binaries with additional components, but did not identify it. He et al. (2016) recently published *BV*-band light curves (LCs), observed in 2004. They obtained a photometric solution with a cool spot on the more massive component. The photometric mass ratio is $q = 0.2556(\pm0.0019)$. They also gave a period decrease rate of $dP/dt = -1.716(\pm002) \times 10^{-7}\,\mathrm{d\,yr^{-1}}$, which results from mass transfer from the more massive component to the less massive one.

GU Ori (= AN 98.1929) was found by Hoffmeister (1930) to be an RRc-type star with a period of 0.68389 d.

Table 1. Observing log, photometric properties, and linear ephemeris.

Variable star	V532 Mon	GU Ori
Comparison star	HD 293068	TYC 738-1071-1
Check star	GSC 4814-1217	TYC 738-2109-1
Exposure time	50 s (*V*); 30 s (*R*)	50 s (*V*); 30 s (*R*)
Observation dates	2011 November 23, 25, 27; 2010 January 20, March 4	2011 January 16, 18, 20, March 16, December 24, 26, 28; 2012 February 1
Telescope	85 cm(XLs); 1.56 m(SHAO)	85 cm(XLs); 60 cm(XLs)
Data number	453 (*V*), 450 (*R*)	796 (*V*), 820 (*R*)
Standard error	± 0.007 mag (*V*), ± 0.006 mag (*R*)	± 0.006 mag (*V*), ± 0.005 mag (*R*)
Amplitude	0.367 mag (*V*), 0.355 mag (*R*)	0.748 mag (*V*), 0.715 mag (*R*)
Max. I–Max. II	–	−0.024 mag (*V*), −0.020 mag (*R*)
Epoch (HJD)	2455919.2865	2455581.9658
Period (d)	0.46698086	0.47067725

Steiner-Sohn (1987) reclassified it to be a W UMa-type eclipsing binary. Samolyk (1985) determined its period to be 0.470681 d, which has been updated to be 0.4706810 d (Hoffmann et al. 2006). Samolyk (1985) suggested that the period of GU Ori had not been constant over the past 50 years. The depth of the primary eclipse is 1.4 mag (Kreiner et al. 2001). This star was still wrongly listed as an EA-type star (Malkov et al. 2006). Hoffmann et al. (2006) studied the third bodies as the cause for orbital period changes. Until now, no extra photometric or spectroscopic information on this star has been reported.

In this paper, we photometrically and spectroscopically observe these two contact binaries, V532 Mon and GU Ori. Multicolor photometric data are reported in subsection 2.1. The spectral observations are presented in subsection 2.2. Orbital period analysis is performed (see section 3). In section 4, we apply detailed LC models. In the final section (section 5), we discuss their possible evolutionary states and give the interpretations of period variations for two eclipsing binaries.

2 Observations

2.1 Photometry

Comprehensive photometry was carried out for V532 Mon and GU Ori from 2010 January to 2013 January, by using the 60 cm telescope (Yang et al. 2010) and 85 cm telescope (Zhou et al. 2009) at Xinglong station (XLs), National Astronomical Observatories of China (NAOC), and the 1.56 m telescope at the Shanghai Astronomical Observatory (SHAO). The standard Johnson–Cousins UBVR$_c$I$_c$ systems were applied. All effective CCD images were reduced by using the IMRED and APPHOT packages in IRAF.[1] After the bias and dark subtraction and the flat-field correction were applied, we deduced the individual magnitudes from each stars. Differential extinction was neglected due to small angular distances between all stars. We then extracted the magnitudes for individual stars and corresponding heliocentric Julian date (HJD) from the observing time for every image. We finally obtained the differential magnitudes ($\Delta m = m_{\rm var} - m_{\rm com}$) between the variable ($m_{\rm var}$) and comparison star ($m_{\rm com}$). The detailed observing log, photometric properties, and linear ephemerides are listed in table 1. The complete LCs for two eclipsing binaries, used in section 4 and shown in figures 1 and 2, are only taken from the 85 cm telescope. Phases are computed using the linear ephemerides in table 1. The individual photometric data (i.e., HJD versus Δm) are listed in table 2.

For V532 Mon, the complete LCs in the *VR* bands are shown in figure 1a. In figure 1b, we plot two LCs in the *V* band which were observed in 2011 November and 2004 January and February (He et al. 2016). An intrinsic small light variability occurs from phase 0.65 to 0.85 in 2004. The light maxima at phase 0.75 is brighter by up to 0.01 mag than the light maxima at phase 0.25. This case may occur in another contact binary, DZ Psc (Yang et al. 2013b), whose asymmetric LCs are modeled by a spot on the primary component.

For another binary, GU Ori, its complete LCs are displayed in figure 2. The almost equal depths for both eclipses indicates that GU Ori is a typical EW-type binary, not an EA-type one (see Kreiner et al. 2001). On 2011 March 16 and 2012 February 1, we observed two total eclipses, which are shown in figure 3. The total eclipse continues with a duration time of ∼30 min. The *VR*-band LCs evidently show the unequal height between both light maxima (i.e., O'Connell effect; Milone 1968; Davidge & Milone 1984). This kind of phenomenon occurs in other active eclipsing binaries, such as DF CVn (Dai et al. 2011) and CK Boo (Yang et al. 2012), which may be modeled by a dark spot.

[1] ⟨http://iraf.noao.edu/⟩.

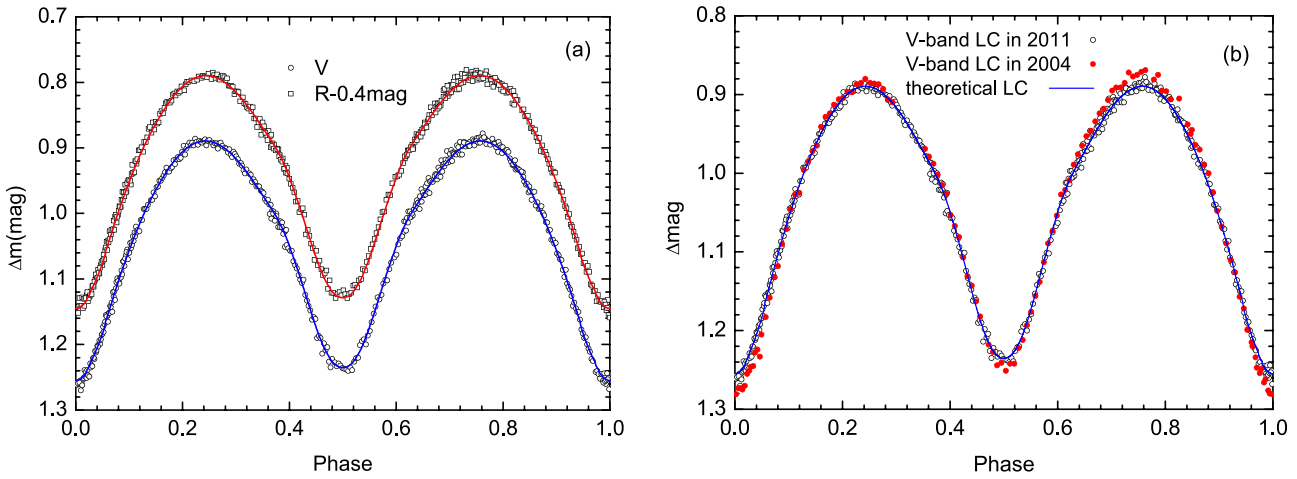

Fig. 1. (a) *VR* LCs for V532 Mon, observed in 2011. (b) Comparing *V*-band LCs in 2011 and in 2004. The data in 2004 is taken from He, Qian, and Soonthornthum (2016), which adds a displacement of −0.08 mag. The theoretical LCs were plotted as the continuous lines in both panels. (Color online)

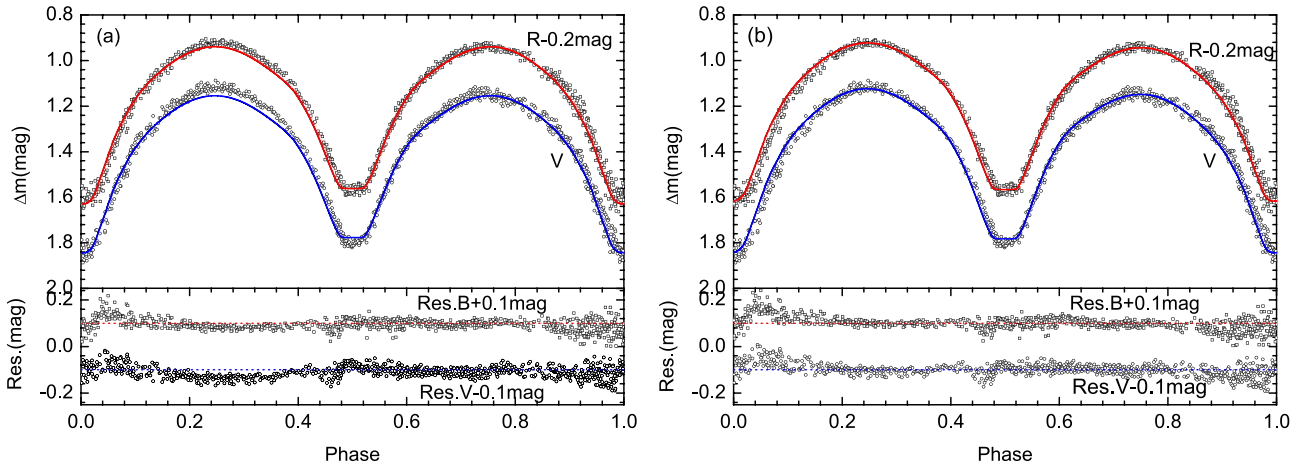

Fig. 2. Entire LCs in *VR* bands for GU Ori, which are modeled by (a) Sol. 1 without a spot and (b) Sol. 2 with a spot. The computed LCs are plotted as dotted and solid lines, respectively. The residuals for LCs, i.e., observed magnitudes minus calculated ones from Sol. 1 and Sol. 2, are also displayed in the lower part of both panels, respectively. (Color online)

2.2 Spectroscopy

The spectra for the two binaries were obtained by using the Yunnan Faint Object Spectrograph and Camera (YFOSC) attached to the 2.4 m telescope at Lijiang Observatory on 2016 December 1 and 9. In the observing process, we chose a 93-mm-long slit, and a *Grism*-3 with wavelength ranging from 3200 Å to 9200 Å. The exposure time is 10 min for each star. Reduction of the spectra was performed by using IRAF packages, including bias subtraction, flat-fielding, and cosmic-ray removal. Finally, the one-dimensional spectrum was extracted. Using the *winmk* software,[2] the normalized spectra are displayed in figure 4. By comparing the spectra of standard stars (Pickles 1998), we estimated the spectral types to be F5V for V532 Mon and G0V for GU Ori.

3 Studying period changes

Eclipse times were monitored for V532 Mon on 2010 January 10 and March 4 with the 1.56 m telescope, and for GU Ori on 2012 February 1 with the 60 cm telescope. Using new observations together with AAVSO data,[3] we obtained several eclipse times, which are listed in table 3. The period variations for V532 Mon have been recently analyzed by He, Qian, and Soonthornthum (2016). Together with our new times of minimum light, we obtained an orbital period decrease rate of $dP/dt = -1.72(\pm0.05) \times 10^{-7}\,\mathrm{d\,yr^{-1}}$, which verified He, Qian, and Soonthornthum's (2016) result.

The orbital period for GU Ori may be variable (Samolyk 1985), which has not been analyzed up to now. Several

[2] ⟨http://www.appstate.edu/~grayro/MK/winmk.htm⟩.

[3] ⟨https://www.aavso.org/sites/default/files/tmp/aavsodata_56bc35d6ab043.txt⟩.

Table 2. *VR*-band observations for V532 Mon and GU Ori.*

Star	*V* band		*R* band	
	JD(Hel.)	Δm	JD(Hel.)	Δm
V532 Mon	2455919.1067	1.012	2455919.1073	1.316
V532 Mon	2455919.1079	1.012	2455919.1086	1.312
V532 Mon	2455919.1092	1.007	2455919.1098	1.304
V532 Mon	2455919.1104	0.997	2455919.1111	1.304
V532 Mon	2455919.1117	0.997	2455919.1123	1.301
V532 Mon	2455919.1129	1.005	2455919.1136	1.295
V532 Mon	2455919.1142	1.003	2455919.1148	1.300
V532 Mon	2455919.1154	0.994	2455919.1161	1.287
GU Ori	2455577.9377	1.551	2455577.9383	1.562
GU Ori	2455577.9405	1.614	2455577.9401	1.635
GU Ori	2455577.9415	1.587	2455577.9410	1.611
GU Ori	2455577.9433	1.629	2455577.9419	1.589
GU Ori	2455577.9451	1.618	2455577.9428	1.620
GU Ori	2455577.9460	1.647	2455577.9437	1.614
GU Ori	2455577.9469	1.669	2455577.9446	1.591
GU Ori	2455577.9478	1.688	2455577.9455	1.629

*The entire table is available in the electronic edition as Supporting Information.

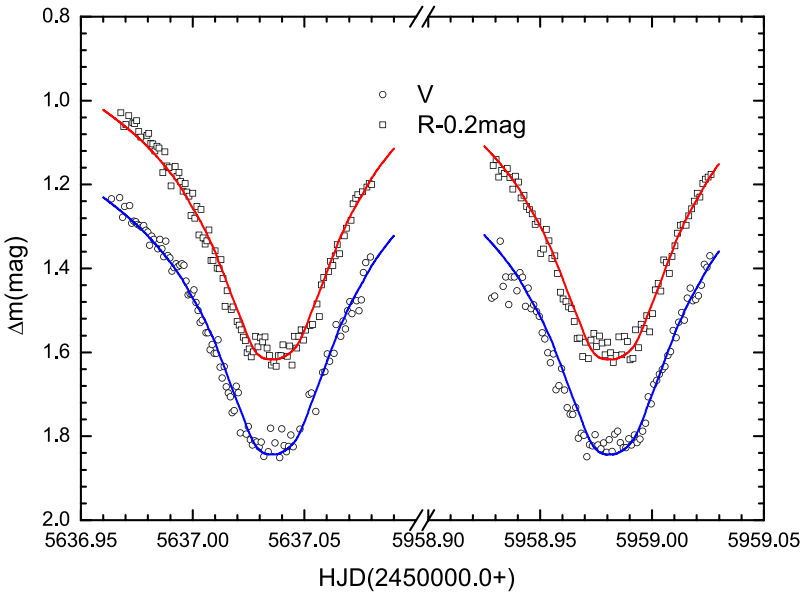

Fig. 3. Two total eclipses, which were observed on 2011 March 16 with the 85 cm telescope, and on 2012 February 1 with the 60 cm telescope, respectively. (Color online)

dozen low-precision measurements (i.e., plate and visual data) from before HJD 2450120.2312 have been published (Safar & Zejda 2000a). However, this part of the $(O-C)$ curve shows large scatter and a long gap from Kreiner et al. (2001).[4] We then collected 128 high-precision results in order to study GU Ori's period changes. Due to the different measurement precision for the eclipsing times, we assign a weight of 1 to plate data, and a weight of 10 to photoelectric/CCD cases.

We assemblea total of 238 eclipsing times, including three photoelectric and 125 CCD results, which are listed in table 4. From those data, we refined a new linear ephemeris as follows:

$$\text{Min.I} = \text{HJD}2455581.9658(\pm 0.0003) + 0.47067725(\pm 0.00000004) \times E \quad (1)$$

[4] ⟨http://www.as.up.krakow.pl/o-c/data/getdata.php3?GU%20ori⟩.

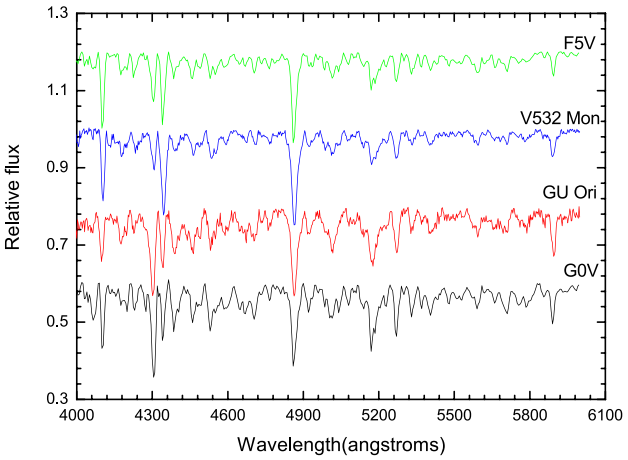

Fig. 4. Spectroscopic observations for V532 Mon and GU Ori. (Color online)

Table 3. New eclipse timings of two contact binaries.

Star	JD (Hel.)	Error	Min.	Filter	Telescope
	2455248.01674	±0.00046	II	*V*	1.56 m
	2455625.09265	±0.00059	I	*V*	1.56 m
	2455919.28645	±0.00020	I	*V*	85 cm
V532 Mon	2455919.28658	±0.00022	I	*R*	85 cm
	2455923.25583	±0.00025	II	*V*	85 cm
	2455923.25552	±0.00022	II	*R*	85 cm
	2455577.96636	±0.00031	II	*V*	85 cm
	2455577.96582	±0.00031	II	*R*	85 cm
	2455581.96801	±0.00039	I	*V*	85 cm
	2455581.96698	±0.00036	I	*R*	85 cm
	2455920.14968	±0.00033	II	*V*	85 cm
	2455920.14982	±0.00029	II	*R*	85 cm
GU Ori	2455958.98210	±0.00023	I	*V*	60 cm
	2455958.98220	±0.00011	I	*R*	60 cm
	2454888.65660	±0.00037	I	*V*	AAVSO
	2454890.77362	±0.00044	I	*V*	AAVSO
	2456272.91661	±0.00172	I	*V*	AAVSO
	2456592.98121	±0.00023	I	*V*	AAVSO
	2456715.59169	±0.00014	II	*V*	AAVSO

The initial $(O-C)_i$ residuals are listed in table 4 and shown in figure 5a. From this figure, the $(O-C)_i$ curve may be described as an upward parabola, showing the existence of a secular period increase. A linear unweighted least-squares method led to the following equation:

$$(O-C)_i = -0.0007(\pm 0.0001) + 8.7(\pm 0.1) \times 10^{-7} \times E + 9.33(\pm 0.06) \times 10^{-11} \times E^2, \quad (2)$$

which is plotted as a solid line in figure 5a. From equation (2), one can determine a rate of period increase, i.e., $dP/dt = +1.45(\pm 0.01) \times 10^{-7}\,\mathrm{d\,yr^{-1}}$. The final residuals $(O-C)_f$ are listed in table 4 and displayed in figure 5b. Although a bit of scatter exists, no regularity is found from the $(O-C)_f$ curve.

4 Analyzing light curves

Modeling LCs for V532 Mon and GU Ori are performed by the 2015 version of the Wilson–Devinney (W-D) software (Wilson & Devinney 1971; Wilson 1979; Wilson & van Hamme 2014), which is commonly used for this purpose.[5] Based on the calibration of MK spectral types (Cox 2000), we estimated an effective mean temperature from the spectral type assumed by an error of a subtype. The temperatures for star 1 (i.e., the more massive component) are $T_1 = 6650(\pm 275)$ K for V532 Mon and $T_1 = 5940(\pm 125)$ K for GU Ori. The gravity darkening coefficients $g_{1,2} = 0.32$ (Lucy 1967) and bolometric albedos $A_{1,2} = 0.5$ (Rucinski 1973) are adopted. The two-parameter logarithmic limb-darkening coefficients were taken from the listed tables (van Hamme 1993; van Hammme & Wilson 2007). Other adjustable parameters are i, q, T_2, Ω_1, Ω_2, and L_1. In the 2015 version of the W-D code, V and R bands correspond to numbers 7 and 15, respectively. We also set KSD = 1, NOISE = 2, N1 = 60, N2 = 60, and IPB = 0.

According to suggestions made by W. van Hamme (2017 private communication), the errors from a least-squares fit are internal to the fit and do not reflect uncertainties in any other chosen parameters that are kept fixed. According to the input error for T_1, we can easily obtain the uncertainty in T_2. Without using radial velocity curves in the W-D code, the mass ratio error for the total eclipse binary can also appear small, in which case q is determined very well from the LCs (Terrell & Wilson 2005). Meanwhile, the error of mass ratio for the partial eclipse binary q is not well determined from LCs alone, and the error, although correct in the formal sense, may not reflect the true "uncertainty" of the parameter. A feasible method is a "q-search" approach, in which we can see how the sum of squared residuals (SSRs) changes with different fixed q-values. A graph of SSRs vs. q will probably show a fairly wide, flat bottom, and the width of that bottom reflects a more realistic uncertainty of q. The errors for other parameters are still adopted to be the output standard errors from the W-D code.

When solving the LCs, a q-search process is performed for a series of solutions. We begin to use *mode 2* (i.e., detached configuration) to model LCs. For some fixed mass ratios, the surface potentials for both components (i.e., Ω_1 and Ω_2) always suffice for the relation $\Omega_{L2} < \Omega_{1,2} < \Omega_{\mathrm{Roche}} = \Omega_{L1}$. We then take *mode 3* (i.e., contact configuration) to obtain the photometric solutions.

[5] Available at ⟨ftp://ftp.astro.ufl.edu/pub/wilson/lcdc2015⟩.

Table 4. Photometric and CCD times of light minima for GU Ori.

JD (Hel.)	Epoch	Method	Min	$(O-C)_i$ (d)	$(O-C)_f$ (d)	Reference*
2450120.2312	−11604.0	CCD	I	+0.0042	+0.0010	(1)
2450138.3520	−11565.5	CCD	II	+0.0039	+0.0008	(1)
2450139.2915	−11563.5	CCD	II	+0.0021	−0.0010	(1)
2450147.2955	−11546.5	CCD	II	+0.0046	+0.0015	(1)
2450163.2988	−11512.5	CCD	II	+0.0048	+0.0017	(1)
2450773.5269	−10216.0	CCD	I	−0.0001	−0.0017	(1)
2450839.4256	−10076.0	CCD	I	+0.0038	+0.0024	(2)
2450863.4275	−10025.0	pe	I	+0.0011	−0.0003	(3)
2450865.3103	−10021.0	pe	I	+0.0012	−0.0001	(3)
2450888.3750	−9972.0	CCD	I	+0.0027	+0.0014	(2)
2450897.3183	−9953.0	pe	I	+0.0032	+0.0019	(3)
2450904.3750	−9938.0	CCD	I	−0.0003	−0.0016	(4)
2451144.1871	−9428.5	CCD	II	+0.0018	+0.0010	(5)
2451144.8938	−9427.0	CCD	I	+0.0024	+0.0016	(5)
2451165.3671	−9383.5	CCD	II	+0.0013	+0.0005	(4)
2451165.6013	−9383.0	CCD	I	+0.0001	−0.0006	(4)
2451176.4278	−9360.0	CCD	I	+0.0011	+0.0004	(4)
2451225.3767	−9256.0	CCD	I	−0.0005	−0.0011	(4)
2451241.3810	−9222.0	CCD	I	+0.0008	+0.0002	(6)
2451481.4266	−8712.0	CCD	I	+0.0010	+0.0008	(6)
2451488.7227	−8696.5	CCD	II	+0.0016	+0.0014	(7)
2451543.5568	−8580.0	CCD	I	+0.0018	+0.0017	(6)
2451544.7311	−8577.5	CCD	II	−0.0006	−0.0007	(7)
2451568.2640	−8527.5	CCD	II	−0.0016	−0.0017	(8)
2451568.4986	−8527.0	CCD	I	−0.0023	−0.0024	(8)
2451571.3231	−8521.0	CCD	I	−0.0019	−0.0020	(8)
2451571.5555	−8520.5	CCD	II	−0.0048	−0.0049	(8)
2451572.2676	−8519.0	CCD	I	+0.0013	+0.0012	(9)
2451585.4456	−8491.0	CCD	I	+0.0003	+0.0003	(9)
2451586.6216	−8488.5	CCD	II	−0.0004	−0.0004	(7)
2451592.2700	−8476.5	CCD	II	−0.0001	−0.0001	(10)
2451602.6253	−8454.5	CCD	II	+0.0003	+0.0003	(7)
2451603.3299	−8453.0	CCD	I	−0.0011	−0.0011	(9)
2451620.2764	−8417.0	CCD	I	+0.0010	+0.0010	(10)
2451626.3930	−8404.0	CCD	I	−0.0012	−0.0012	(11)
2451799.6057	−8036.0	CCD	I	+0.0023	+0.0026	(11)
2451881.7348	−7861.5	CCD	II	−0.0018	−0.0014	(7)
2451898.4460	−7826.0	CCD	I	+0.0004	+0.0008	(10)
2451912.5648	−7796.0	CCD	I	−0.0012	−0.0008	(7)
2451923.3900	−7773.0	CCD	I	−0.0015	−0.0011	(10)
2451924.3332	−7771.0	CCD	I	+0.0003	+0.0007	(12)
2451956.3386	−7703.0	CCD	I	−0.0003	+0.0002	(10)
2452209.5612	−7165.0	CCD	I	−0.0021	−0.0014	(10)
2452279.4571	−7016.5	CCD	II	−0.0018	−0.0010	(8)
2452312.6396	−6946.0	CCD	I	−0.0020	−0.0012	(7)
2452321.3465	−6927.5	CCD	II	−0.0027	−0.0019	(10)
2452337.5850	−6893.0	CCD	I	−0.0025	−0.0016	(7)
2452609.8730	−6314.5	CCD	II	−0.0013	−0.0002	(7)
2452610.8135	−6312.5	CCD	II	−0.0022	−0.0011	(7)
2452619.5214	−6294.0	CCD	I	−0.0018	−0.0007	(13)
2452625.8747	−6280.5	CCD	II	−0.0026	−0.0015	(7)
2452662.5902	−6202.5	CCD	II	+0.0000	+0.0011	(7)
2452669.6486	−6187.5	CCD	II	−0.0017	−0.0006	(7)
2452672.4735	−6181.5	CCD	II	−0.0009	+0.0002	(12)

Table 4. (Continued)

JD (Hel.)	Epoch	Method	Min	$(O-C)_i$ (d)	$(O-C)_f$ (d)	Reference*
2452683.2996	−6158.5	CCD	II	−0.0004	+0.0007	(12)
2452694.3594	−6135.0	CCD	I	−0.0015	−0.0004	(12)
2452695.3018	−6133.0	CCD	I	−0.0004	+0.0007	(12)
2452701.6544	−6119.5	CCD	II	−0.0020	−0.0009	(7)
2452723.3060	−6073.5	CCD	II	−0.0015	−0.0004	(12)
2452981.4722	−5525.0	CCD	I	−0.0018	−0.0005	(14)
2452983.3557	−5521.0	CCD	I	−0.0010	+0.0003	(12)
2452983.5922	−5520.5	CCD	II	+0.0002	+0.0015	(12)
2453035.6009	−5410.0	CCD	I	−0.0010	+0.0003	(15)
2453047.1311	−5385.5	CCD	II	−0.0024	−0.0011	(16)
2453314.9481	−4816.5	CCD	II	−0.0007	+0.0006	(15)
2453323.8904	−4797.5	CCD	II	−0.0013	+0.0000	(15)
2453368.6039	−4702.5	CCD	II	−0.0021	−0.0008	(15)
2453408.1395	−4618.5	CCD	II	−0.0034	−0.0021	(17)
2453409.3196	−4616.0	CCD	I	+0.0000	+0.0013	(18)
2453411.2039	−4612.0	CCD	I	+0.0016	+0.0029	(17)
2453413.7883	−4606.5	CCD	II	−0.0027	−0.0014	(15)
2453435.6774	−4560.0	CCD	I	−0.0001	+0.0012	(15)
2453445.3257	−4539.5	CCD	II	−0.0007	+0.0006	(18)
2453674.5457	−4052.5	CCD	II	−0.0005	+0.0008	(18)
2453717.3759	−3961.5	CCD	II	−0.0020	−0.0007	(19)
2453735.7347	−3922.5	CCD	II	+0.0004	+0.0017	(15)
2453763.7384	−3863.0	CCD	I	−0.0012	+0.0001	(15)
2454061.9119	−3229.5	CCD	II	−0.0017	−0.0006	(20)
2454091.3295	−3167.0	CCD	I	−0.0014	−0.0003	(21)
2454091.5641	−3166.5	CCD	II	−0.0022	−0.0011	(21)
2454105.6856	−3136.5	CCD	II	−0.0010	+0.0001	(20)
2454107.5678	−3132.5	CCD	II	−0.0015	−0.0004	(20)
2454107.8033	−3132.0	CCD	I	−0.0014	−0.0003	(20)
2454143.1051	−3057.0	CCD	I	−0.0003	+0.0008	(22)
2454165.6978	−3009.0	CCD	I	−0.0002	+0.0009	(20)
2454179.5823	−2979.5	CCD	II	−0.0006	+0.0005	(20)
2454185.7023	−2966.5	CCD	II	+0.0006	+0.0017	(20)
2454380.5621	−2552.5	CCD	II	+0.0000	+0.0009	(23)
2454476.3446	−2349.0	CCD	I	−0.0003	+0.0005	(24)
2454476.5794	−2348.5	CCD	II	−0.0009	−0.0001	(24)
2454496.5837	−2306.0	CCD	I	−0.0004	+0.0004	(25)
2454500.3478	−2298.0	CCD	I	−0.0017	−0.0009	(24)
2454505.2898	−2287.5	CCD	II	−0.0018	−0.0010	(26)
2454520.5873	−2255.0	CCD	I	−0.0013	−0.0005	(25)
2454526.7072	−2242.0	CCD	I	−0.0002	+0.0006	(27)
2454800.8748	−1659.5	CCD	II	−0.0021	−0.0016	(28)
2454845.3560	−1565.0	CCD	I	+0.0001	+0.0005	(29)
2454846.0629	−1563.5	CCD	II	+0.0010	+0.0014	(30)
2454877.5967	−1496.5	CCD	II	−0.0006	−0.0002	(31)
2454888.6566	−1473.0	CCD	I	−0.0016	−0.0012	(17)
2454890.7736	−1468.5	CCD	II	−0.0027	−0.0023	(17)
2454905.6039	−1437.0	CCD	I	+0.0013	+0.0017	(32)
2455114.8208	−992.5	CCD	II	+0.0022	+0.0023	(32)
2455156.7104	−903.5	CCD	II	+0.0015	+0.0015	(32)
2455206.6022	−797.5	CCD	II	+0.0015	+0.0014	(32)
2455210.6022	−789.0	CCD	I	+0.0008	+0.0007	(32)
2455253.6686	−697.5	CCD	II	+0.0002	+0.0001	(32)
2455262.6120	−678.5	CCD	II	+0.0007	+0.0006	(33)

Table 4. (Continued)

JD (Hel.)	Epoch	Method	Min	$(O-C)_i$ (d)	$(O-C)_f$ (d)	Reference*
2455263.5537	−676.5	CCD	II	+0.0011	+0.0010	(33)
2455566.6698	−32.5	CCD	II	+0.0010	+0.0003	(34)
2455575.6091	−13.5	CCD	II	−0.0026	−0.0033	(35)
2455577.9661	−8.5	CCD	II	+0.0011	+0.0004	(17)
2455581.9680	+0.0	CCD	I	+0.0022	+0.0015	(17)
2455631.6244	+105.5	CCD	II	+0.0022	+0.0014	(34)
2455896.8518	+669.0	CCD	I	+0.0029	+0.0016	(36)
2455920.1498	+718.5	CCD	II	+0.0024	+0.0010	(17)
2455921.7978	+722.0	CCD	I	+0.0030	+0.0016	(37)
2455958.9822	+801.0	CCD	I	+0.0039	+0.0025	(17)
2455964.6296	+813.0	CCD	I	+0.0032	+0.0018	(38)
2455981.3356	+848.5	CCD	II	+0.0002	−0.0013	(38)
2456217.8540	+1351.0	CCD	I	+0.0032	+0.0012	(38)
2456221.8536	+1359.5	CCD	II	+0.0021	+0.0001	(38)
2456256.9186	+1434.0	CCD	I	+0.0016	−0.0005	(39)
2456272.9166	+1468.0	CCD	I	−0.0034	−0.0056	(17)
2456309.6355	+1546.0	CCD	I	+0.0027	+0.0004	(40)
2456325.6381	+1580.0	CCD	I	+0.0022	−0.0001	(40)
2456592.9812	+2148.0	CCD	I	+0.0007	−0.0023	(17)
2456715.5916	+2408.5	CCD	II	−0.0004	−0.0037	(17)

*References: (1) Safar and Zejda (2000a); (2) Safar and Zejda (2000b); (3) Agerer, Dahm, and Hubscher (1999); (4) Agerer, Dahm, and Hubscher (2001); (5) Baldwin (1999); (6) Safar and Zejda (2002); (7) Baldwin (2003); (8) Agerer and Hubscher (2002); (9) B.R.N.O. Observers (2002); (10) Brát, Zejda, and Svoboda (2007); (11) Zejda (2002); (12) Zejda (2004); (13) Agerer and Hubscher (2003); (14) Kotkova and Wolf (2006); (15) Baldwin and Samolyk (2006); (16) Krajci (2005); (17) present work; (18) Zejda, Mikulasek, and Wolf (2006); (19) Hubshcer, Paschke, and Walter (2006); (20) Baldwin and Samolyk (2007); (21) Hubscher and Walter (2007); (22) Nagai (2008); (23) Borkovits et al. (2008); (24) Hubscher, Steinbach, and Walter (2009); (25) Samolyk (2008a); (26) Diethelm (2008); (27) Samolyk (2008b); (28) Diethelm (2009); (29) Hubscher et al. (2010); (30) Nagai (2010); (31) Samolyk (2009); (32) Samolyk (2010); (33) Samolyk (2011a); (34) Samolyk (2011b); (35) Diethelm (2011); (36) Diethelm (2012); (37) Samolyk (2012); (38) Samolyk (2013a); (39) Diethelm (2013); (40) Samolyk (2013b).

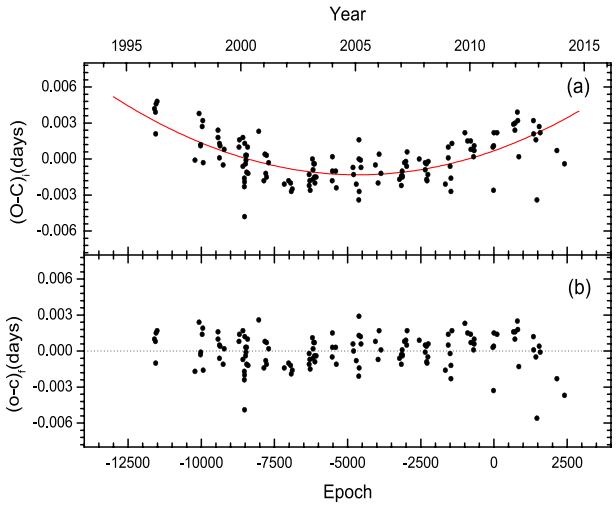

Fig. 5. The $(O-C)$ diagram for GU Ori. The red continuous line is plotted by equation (2). The filled circles represent photoelectric or CCD measurements. (Color online)

The SSRs(q *versus* Σ) are displayed in figure 6. The Σ-curve first abruptly decreases and then slowly increases with increasing mass ratio. Although small oscillations occur, the minimum values of Σ apparently exist around $q = 0.19$ for V532 Mon and $q = 0.45$ for GU Ori. This indicates that two stars are A-subtype contact binaries. Other details are given as follows.

(1) For V532 Mon, the depths for the primary and secondary eclipses are almost equal, which implies that their temperature difference may be very small. After $q = 0.19$ is considered to be an adjustable parameter, we deduced the photometric solution, which is listed in table 6. The computed LCs are displayed as solid lines in figure 1. The fill-out factor is $f = 43.7(\pm0.9)\%$. The error for the mass ratio is estimated to be ±0.006 from figure 6 a from $q = 0.18$ to $q = 0.30$. From figure 4 of He, Qian, and Soonthornthum (2016), the error for mass ratio may be ±0.06 from $q = 0.20$ to $q = 0.32$, which is based on the sum of squared residuals. Therefore, the error may be greatly underestimated. Their photometric solution is largely different from our solution. The mains reason for this may result from their small data

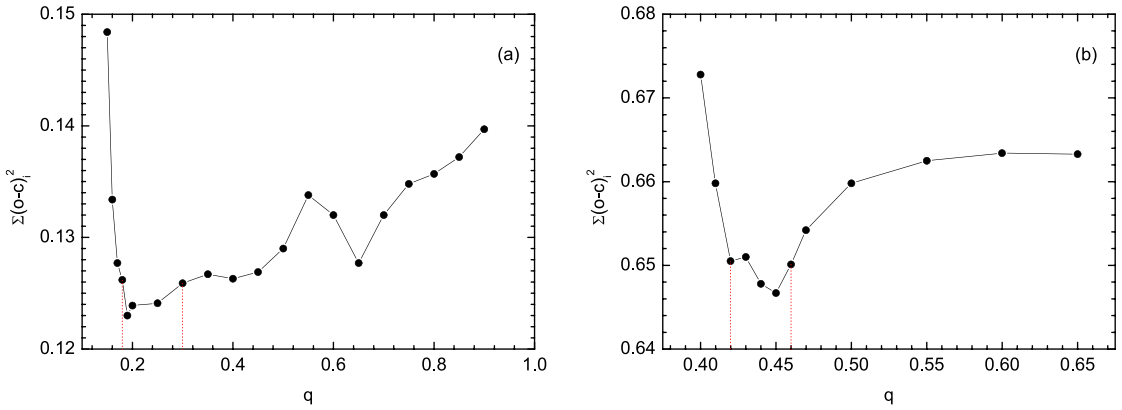

Fig. 6. Sum of squared residuals (Σ versus q) for V532 Mon (a) and GU Ori (b). (Color online)

points, which may cause the variable amplitude to be large, as seen from figure 1b. The observational data also do not cover the entire phase, with a gap present from phase 0.30 to phase 0.35. From figure 1b, the variation of LC in the V band may occur in Max. II (i.e., phase of 0.75), which may be appropriate for a model with a hot spot instead of a cool one He, Qian, and Soonthornthum (2016). Moreover, the mass transfer from the secondary to the primary may produce a hot spot on the more massive component due to the orbital period decrease.

(2) GU Ori is an EW-type binary with a total eclipse around phase 0.5. Its mass ratio, derived from the LC alone, may be more reliable (Terrell & Wilson 2005). The uncertainty in mass ratio is chosen to be ± 0.02 from $q = 0.42$ to $q = 0.46$, which is larger than the output standard error from the W-D code. The initial value of $q = 0.45$ was treated as a free parameter. After some iterations, we obtained the photometric solution (Sol. 1 without spot), which is listed in table 5. The corresponding theoretical LCs from Sol. 1 are displayed in figure 2a. The residuals, i.e., the observed

Table 5. Photometric elements for two contact binaries.

Parameter	V532 Mon	GU Ori	
		Sol. 1 without spot	Sol. 2 with spot
i (°)	71.6(±0.1)	86.2(±0.4)	86.1(±0.7)
$q = M_2/M_1$	0.190(±0.006)	0.455(±0.020)	0.455(±0.020)
T_1(K)	6650(±275)	5940(±125)	
X_1, Y_1	0.644, 0.243	0.649, 0.218	
x_{1V}, y_{1V}	0.703, 0.287	0.751, 0.253	
x_{1R}, y_{1R}	0.631, 0.289	0.680, 0.266	
T_2(K)	6575(±271)	5910(±124)	6003(±119)
X_2, Y_2	0.645, 0.242	0.649, 0.216	0.649, 0.221
x_{2V}, y_{2V}	0.707, 0.286	0.753, 0.250	0.747, 0.259
x_{2R}, y_{2R}	0.635, 0.288	0.661, 0.262	0.655, 0.268
$\Omega_1 = \Omega_2$	2.1546(±0.0009)	2.7146(±0.0041)	2.7146(±0.0037)
$L_1/(L_1 + L_2)_V$	0.8162(±0.0009)	0.6733(±0.0017)	0.6584(±0.0015)
$L_1/(L_1 + L_2)_R$	0.8151(±0.0008)	0.6724(±0.0016)	0.6600(±0.0014)
r_1 (pole)	0.5041(±0.0008)	0.4359(±0.0015)	0.4344(±0.0016)
r_1 (side)	0.5542(±0.0009)	0.4674(±0.0022)	0.4653(±0.0022)
r_1 (back)	0.5807(±0.0012)	0.5010(±0.0020)	0.4979(±0.0032)
r_2 (pole)	0.2449(±0.0013)	0.3081(±0.0024)	0.3064(±0.0022)
r_2 (side)	0.2570(±0.0015)	0.3238(±0.0028)	0.3218(±0.0028)
r_2 (back)	0.3066(±0.0036)	0.3680(±0.0045)	0.3649(±0.0054)
ϕ (°)	–	–	90.0
θ (°)	–	–	59.0(±3.3)
γ (°)	–	–	20.9(±1.5)
T_s/T	–	–	0.93(±0.10)
$\Sigma(o-c)^2$	0.1128	0.6029	0.4831
f (%)	43.7(±0.9)	26.9(±1.5)	26.9(±1.3)

Table 6. Preliminary absolute parameters for the two binaries.

Parameter	V532 Mon	GU Ori
Spectral type	F5V	G0V
a ($R_\odot$)	3.00±0.05	2.93±0.06
M_1 ($M_\odot$)	1.40±0.06	1.05±0.05
M_2 ($M_\odot$)	0.27±0.02	0.47±0.02
R_1 ($R_\odot$)	1.64±0.08	1.36±0.09
R_2 ($R_\odot$)	0.81±0.04	0.97±0.07
L_1 ($L_\odot$)	4.70±0.47	2.07±0.27
L_2 ($L_\odot$)	1.09±0.12	1.09±0.15

minus computed values, are displayed in its lower panel. The LCs could not be fitted from phase 0.2 to phase 0.4. Max. I at phase 0.25 is brighter than Max. II at phase 0.75 by up to ∼0.02 mag (table 1). The LCs for GU Mon show unequal light maxima, i.e., the existence of the O'Connell effect (Milone 1968). For the star with a spectral type of G0V-type binary, magnetic activity occurs in this solar-type star. Supposing that a cool spot is located on the equator of the more massive component (i.e., $\phi = 90^\circ$), we finally obtained the spotted solution (i.e., Sol. 2) listed in table 6. The computed LCs from Sol. 2 are plotted as solid lines in the upper panel of figure 2b. The corresponding LC residuals are also displayed, in the figure's lower panel. Although there is some discrepancy between observed and computed LCs, especially around phases 0.05 and 0.46, all observations can generally be fitted well. As displayed in figure 6, two eclipses, observed on 2011 March 16 and 2012 February 1, were fitted well except for a bit of scatter in some observational points.

5 Discussion

5.1 Absolute parameters and evolutionary status

Due to the lack of spectroscopic elements (i.e., the semi-amplitudes of radial velocity curves, K_1 and K_2), the absolute parameters for the two binaries are estimated by using Kepler's third law, $M_1 + M_2 = 0.134a^3/P^2$, in which $M_{1,2}$, a, and P are in units of $M_\odot$, $R_\odot$, and d, respectively. From the spectral type assumed with an error in the subtype (see subsection 2.2), the mass of the primary can be estimated from the tables of Cox (2000). The derived masses are $M_1 = 1.40(\pm0.06)\,M_\odot$ for V532 Mon and $M_1 = 1.05(\pm0.05)\,M_\odot$ for GU Ori. Combining with photometric solutions, we can derive other parameters by using the formula $L \propto R^2T^4$. The absolute parameters are listed in table 6. Figure 7 displays both components in the H-R diagram, in which ZAMS (zero-age main sequence) and TAMS (terminal-age main sequence) (as solid lines) are plotted, and evolutionary tracks for solar chemical compositions (as dotted lines) are taken from Girardi et al. (2000).

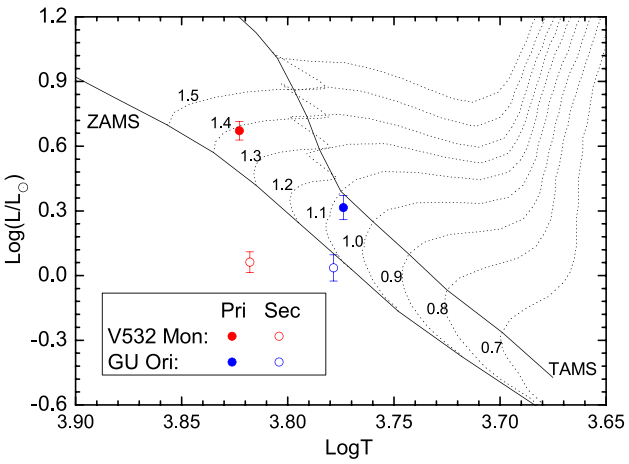

Fig. 7. Both components for the two binaries in the temperature–luminosity diagram. (Color online)

For a low-mass star, there is a discrepancy between the observation and theory (Hoxie 1973). López-Morales and Shaw (2007) concluded that the models underestimate the radii of low-mass stars by at least 10%, which agrees with the results from Feiden and Dotter (2013). The uncertainty for the stellar luminosity is thus at least 20%. For the contact binaries with short periods (∼1 d), the rotational period has been synchronized with its orbital period due to the tidal interaction (Zahn 1977). The components rotate faster than a comparable single field star because the stellar dynamo mechanism is largely driven by rotation. This kind of tidal synchronization for binaries allows a star to produce and maintain a strong magnetic field. The internal magnetic field may result in its radius being inflated (Feiden & Chaboyer 2013).

From figure 7, the primary and secondary components for GU Ori lie near the TAMS line and the ZAMS line, which indicates that the primary is an evolved main-sequence (MS) star, while the secondary may also be an MS one. For V532 Mon, the primary component is situated between the ZAMS and TAMS lines, which implies that it is a somewhat evolved MS star. The secondary component lies far below the ZAMS line. It may be an M4-type dwarf star with a mass of 0.27 $M_\odot$ (Cox 2000). This kind of discrepancy between observation and theory is similar to that of another eclipsing binary, VZ Cep (Torres & Lacy 2009).

5.2 Interpreting orbital period changes

From equations (1) and (3), the orbital periods for the two binaries show long-term period variations; period decrease for V532 Mon and period increase for GU Mon. This kind of long-term period change occurs in many other contact binaries, such as DZ Psc (Yang et al. 2013b), BL Leo and V1918 Cyg (Yang et al. 2013a), DK Cyg (Lee et al. 2015),

V508 Oph (Xiang et al. 2015), and XZ Leo (Luo et al. 2015). Secular period variations in contact binaries may be generally interpreted by the mass transfer between both components. Considering the conserved mass transfer (i.e., $\dot{M}_1 + \dot{M}_2 = 0$), the transfer rate is computed by the equation (Singh & Chaubey 1986)

$$\frac{\dot{M}_1}{M_1} = \frac{q}{3(1-q)}\frac{\dot{P}}{P}, \tag{3}$$

where M_1 and q refer to the primary's mass and mass ratio, respectively. Inserting the values of $\dot{P}$, P and M_1 into equation (3), we can determine the mass transfer rates, which are $\dot{M}_1 = -4.03(\pm 0.11) \times 10^{-8}\, M_\odot\, \mathrm{yr}^{-1}$ for V532 Mon and $\dot{M}_1 = +8.65(\pm 0.59) \times 10^{-8}\, M_\odot\, \mathrm{yr}^{-1}$ for GU Ori. For GU Mon, the period increase can be interpreted by the "secondary-to-primary" mass transfer. The increasing mass ratio results in the inflation of inner and outer critical Lagrangian surfaces. This will cause the fill-out factor to decrease. Finally, GU Mon may evolve into a broken-contact configuration. V532 Mon with decreasing period will evolve into a deep-contact configuration (see He et al. 2016). This kind of contact binary with secular period changes may provide observational evidence for thermal relaxation oscillation models (Lucy 1976; Flannery 1976; Robertson & Eggleton 1977). In the future, the radial velocity curves and eclipsing times for these two stars are needed to determine absolute parameters and to identify period variations and possible evolutionary states.

Acknowledgements

The authors would like to express many thanks to the anonymous referee for their positive comments. This research is partly supported by the Natural Science Foundation of China (grant Nos. 11473009, U1231102, and U1431114), and the Natural Science Research Project of Anhui Provincial Department of Education (grant No. KJ2017A850). Dr Yuangui Yang thanks Dr James Wicker at RAA of NAOC, who helped us in improving the English of this manuscript. We also thank Professor J. Kreiner for sending all eclipse timings of V532 Mon and GU Mon. The spectrums were observed by using the 2.4-m telescope at the Lijiang station of YNAO. New photometric data was obtained using the 60 cm and 85 cm telescopes at XLs of NAOC and the 1.56-m telescope at SHAO.

Supporting Information

Supplementary data are available at *PASJ* online.

Complete listing of table 2.

References

Agerer, F., Dahm, M., & Hubscher, J. 1999, IBVS, 4712, 1
Agerer, F., Dahm, M., & Hubscher, J. 2001, IBVS, 5017, 1
Agerer, F., & Hubscher, J. 1996, IBVS, 4383, 1
Agerer, F., & Hubscher, J. 2002, IBVS, 5296, 1
Agerer, F., & Hubscher, J. 2003, IBVS, 5484, 1
Baldwin, M. E. 1999, Obs. Min. Timings Ecl. Bin., 5, 1
Baldwin, M. E. 2003, Obs. Min. Timings Ecl. Bin., 8, 1
Baldwin, M., & Samolyk, G. 2006, Obs. Min. Timings Ecl. Bin., 11, 1
Baldwin, M., & Samolyk, G. 2007, Obs. Min. Timings Ecl. Bin., 12, 1
Borkovits, T., et al. 2008, IBVS, 5835, 1
Brát, L., Zejda, M., & Svoboda, P. 2007, Open Eur. J. Var. Stars, 74, 1
B.R.N.O. Observers. 2002, Brno Contr., 32, 4
Cox, A. N. ed. 2000, Allen's Astrophysical Quantities, 4th ed. (New York: Springer)
Dai, H.-F., Yang, Y.-G., & Yin, X.-G. 2011, New Astron., 16, 173
Davidge, T. J., & Milone, E. F. 1984, ApJS, 55, 571
Diethelm, R. 2008, IBVS, 5837, 1
Diethelm, R. 2009, IBVS, 5871, 1
Diethelm, R. 2011, IBVS, 5992, 1
Diethelm, R. 2012, IBVS, 6011, 1
Diethelm, R. 2013, IBVS, 6042, 1
Feiden, G. A., & Chaboyer, B. 2013, ApJ, 779, 183
Feiden, G. A., & Dotter, A. 2013, ApJ, 765, 86
Flannery, B. P. 1976, ApJ, 205, 217
Girardi, L., Bressan, A., Bertelli, G., & Chiosi, C. 2000, A&AS, 141, 371
He, J.-J., Qian, S.-B., & Soonthornthum, B. 2016, AJ, 152, 120
Hoffman, D. I., Harrison, T. E., McNamara, B. J., Vestrand, W. T., Holtzman, J. A., & Barker, T. 2006, AJ, 132, 2260
Hoffmeister, C. 1930, Astron. Nachr., 238, 17
Hoxie, D. T. 1973, A&A, 26, 437
Hubscher, J., Lehmann, P. B., Monninger, G., Steinbach, H.-M., & Walter, F. 2010, IBVS, 5918, 1
Hubscher, J., Paschke, A., & Walter, F. 2006, IBVS, 5731, 1
Hubscher, J., Steinbach, H.-M., & Walter, F. 2009, IBVS, 5874, 1
Hubscher, J., & Walter, F. 2007, IBVS, 5761, 1
Kotkova, L., & Wolf, M. 2006, IBVS, 5676, 1
Krajci, T. 2005, IBVS, 5592, 1
Kreiner, J. M. 2004, Acta Astron., 54, 207
Kreiner, J. M., Kim, C.-H., & Nha, I.-S. 2001, An Atlas of O-C Diagrams of Eclipsing Binary Stars (Cracow: Wydawnictwo Naukowe Akademii Pedagogicznej)
Kukarkin, B. V., et al. 1968, IBVS, 311, 1
Lee, J.-W., Youn, J.-H., Park, J-H., & Wolf, M. 2015, AJ, 149, 194
López-Morales, M., & Shaw, J. S. 2007, ASP Conf. Ser., 362, 26
Lucy, L. B. 1967, Z. Astrophys., 65, 89
Lucy, L. B. 1976, ApJ, 205, 208
Luo, C. Q., Zhang, X. B., Deng, L., Wang, K., & Luo, Y. 2015, AJ, 150, 70
Malkov, O. Y., Oblak, E., Snegireva, E. A., & Torra, J. 2006, A&A, 446, 785
Milone, E. F. 1968, AJ, 73, 708
Nagai, K. 2008, Var. Star Bull. Japan, 46, 1
Nagai, K. 2010, Var. Star Bull. Japan, 50, 1
Pickles, A. J. 1998, PASP, 110, 863
Pribulla, T., Kreiner, J. M., & Tremko, J. 2003, Contr. Astron. Obs. Skalnate Pleso, 33, 38
Pribulla, T., & Rucinski, S. M. 2006, AJ, 131, 2986

Robertson, J. A., & Eggleton, P. P. 1977, MNRAS, 179, 359
Ruciński, S. M. 1973, Acta Astron., 23, 79
Safar, J., & Zejda, M. 2000a, IBVS, 4887, 1
Safar, J., & Zejda, M. 2000b, IBVS, 4888, 1
Safar, J., & Zejda, M. 2002, IBVS, 5263, 1
Samolyk, G. 1985, J. Am. Assoc. Variable Star Obs., 14, 12
Samolyk, G. 2008a, J. Am. Assoc. Variable Star Obs., 36, 171
Samolyk, G. 2008b, J. Am. Assoc. Variable Star Obs., 36, 186
Samolyk, G. 2009, J. Am. Assoc. Variable Star Obs., 37, 44
Samolyk, G. 2010, J. Am. Assoc. Variable Star Obs., 38, 183
Samolyk, G. 2011a, J. Am. Assoc. Variable Star Obs., 39, 94
Samolyk, G. 2011b, J. Am. Assoc. Variable Star Obs., 39, 177
Samolyk, G. 2012, J. Am. Assoc. Variable Star Obs., 40, 975
Samolyk, G. 2013a, J. Am. Assoc. Variable Star Obs., 41, 122
Samolyk, G. 2013b, J. Am. Assoc. Variable Star Obs., 41, 328
Singh, M., & Chaubey, U. S. 1986, Ap&SS, 124, 389
Steiner-Sohn, R. 1987, Mitt. Veränderliche Sterne, 11, 61
Terrell, D., & Wilson, R. E. 2005, Ap&SS, 296, 221
Torres, G., & Lacy, C. H. S. 2009, AJ, 137, 507
van Hamme, W. 1993, AJ, 106, 2096
van Hamme, W., & Wilson, R. E. 2007, ApJ, 661, 1129
Wachmann, A. A. 1966, Astron. Abh. Hamburger Sternw., 7, 339
Wilson, R. E. 1979, ApJ, 234, 1054
Wilson, R. E., & Devinney, E. J. 1971, ApJ, 166, 605
Wilson, R. E., & van Hamme, W. 2014, ApJ, 780, 151
Xiang, F.-Y., Yu, Y.-X., & Xiao, T.-Y. 2015, AJ, 149, 62
Yang, Y.-G., Dai, H.-F., & Yin, X.-G. 2010, New Astron., 15, 392
Yang, Y.-G., Qian, S.-B., & Dai, H.-F. 2013a, AJ, 146, 60
Yang, Y.-G., Qian, S.-B., & Soonthornthum, B. 2012, AJ, 143, 122
Yang, Y.-G., Qian, S.-B., Zhang, L.-Y., Dai, H.-F., & Soonthornthum, B. 2013b, AJ, 146, 35
Zahn, J.-P. 1977, A&A, 57, 383
Zejda, M. 2002, IBVS, 5287, 1
Zejda, M. 2004, IBVS, 5583, 1
Zejda, M., Mikulasek, Z., & Wolf, M. 2006, IBVS, 5741, 1
Zhou, A.-Y., Jiang, X.-J., Zhang, Y.-P., & Wei, J.-Y. 2009, Res. Astron. Astrophys., 9, 349